

Photocatalytic and photoluminescence studies of La, Ce and Dy co-doped ZnO nanoflowers

Syed Irtiqah and Atikur Rahman*

Department of Metallurgical and Materials Engineering, National Institute of Technology
Srinagar, Hazratbal, Srinagar-190006, India

*Corresponding author: atikurrhmn@gmail.com, atikurrhmn@nitsri.net

Ph. no.: 0091-194-2429429

Fax: 0091-194-2420475

Abstract

In the present work, ZnO nanoparticles were doped with varying concentration of Lanthanum (La), Cerium (Ce) and Dysprosium (Dy) using a simple and cost effective co-precipitation approach at low temperatures. The resulting powders were calcined at 500 °C for 1 hour using a muffle furnace, to produce La, Ce, Dy co-doped ZnO nanoparticles with varying stoichiometry viz. $\text{Zn}_{0.97}\text{La}_{0.01}\text{Ce}_{0.01}\text{Dy}_{0.01}\text{O}$, $\text{Zn}_{0.94}\text{La}_{0.02}\text{Ce}_{0.02}\text{Dy}_{0.02}\text{O}$, $\text{Zn}_{0.91}\text{La}_{0.03}\text{Ce}_{0.03}\text{Dy}_{0.03}\text{O}$, $\text{Zn}_{0.88}\text{La}_{0.04}\text{Ce}_{0.04}\text{Dy}_{0.04}\text{O}$ and $\text{Zn}_{0.85}\text{La}_{0.05}\text{Ce}_{0.05}\text{Dy}_{0.05}\text{O}$. This is a simple approach for doping and doesn't require and complex equipment, harmful chemical or sophisticated machinery. The synthesized powders were characterized using X-Ray diffraction (XRD) and Scanning electron microscopy (SEM) for studying the structure, purity, and grain morphology. The average particle size was calculated using XRD and was found to be 35 nm, it also indicated a hexagonal wurtzite structure with no secondary peaks. A change in morphology from nanorods to nanoflowers was observed as the concentration of dopants increased. Photoluminescence (PL) spectra indicated a red shift in the absorption edge towards the visible region of solar spectrum

and this was further confirmed by Diffuse Reflectance Spectra (DRS). The photocatalytic properties of undoped and La, Ce, Dy co-doped ZnO nanoparticles were observed by examining the photodegradation of Rhodamine B dye under UV irradiation. Elimination of dye color indicated the total degradation of organic molecule. The results revealed that ZnO photocatalyst with La, Ce, Dy co-doping concentration $\text{Zn}_{0.85}\text{La}_{0.05}\text{Ce}_{0.05}\text{Dy}_{0.05}\text{O}$ exhibited the best photocatalytic performance (95%) as compared to undoped ZnO. The improved photocatalytic performance can be attributed to the increased surface oxygen vacancies and adsorption capacity. Delay in recombination of charge carriers due to creation trap states in the bandgap of ZnO further improves the photocatalytic performance of doped samples.

Keywords: ZnO; La, Ce, Dy, co-doping; co-precipitation; photoluminescence; photocatalyst; rhodamine B; rare earths

Introduction.

In present times the advancement in electronics and technology can be credited to the semiconductor nanomaterials. Amongst the semiconductor nanomaterials, TiO_2 , ZnS, ZnSe, ZnO, CdSe, indium tin oxide (ITO) etc exhibit excellent optical properties [1]. ZnO being a class II-VI semiconductor, has a wide bandgap (3.37 eV), high binding energy at room temperature, better chemical stability and very high melting point (1975 °C). Owing to its unique properties ZnO is the most commonly used semiconductor in optoelectronic applications viz. photocatalysis, photoluminescence, solar cells, field emission displays etc. Wide scale use of ZnO can be further attributed to its low cost, simple synthesis, little toxicity, electron transport capability and less crystallization temperature [2-7].

Doping i.e. incorporation of small quantity of impurity ions into the host lattice can tune and modify the properties of semiconductors to suit particular applications [8-12]. Optoelectronic and magnetic properties of ZnO can be easily modulated by doping. Among the materials used for doping, rare earth ions with $4f$ configuration have gained maximum attention due to their unique luminescence and recombination sites for the electron hole pairs [13].

Semiconductors used as photocatalysts such as ZnO are crucial in easing the global concerns regarding waste water treatment. Water pollution and the scarcity of water induced by it are the major concerns of the scientific world today. Textile industry and dye production/ utilization units are the major contributors towards the water pollution. Large amounts of effluent water containing intense colored toxic dyes are produced by these every day. Rhodamine B dye owing to its high stability and low cost is the most commonly used dye in the textile industry and dye production units. However it is carcinogenic and mutagenic in nature and hence extremely harmful for human and aquatic life. So degradation of Rhodamine B dye is pivotal in waste water treatment, conservation of aquatic life and human safety [14]. Photocatalysis has evolved as an efficient, cost effective and environment friendly method for waste water treatment. Semiconductor nanomaterials like TiO_2 , ZnS, ZnO are suitable candidates for photocatalysis, however ZnO is the most commonly used owing to its low cost, inertness to chemicals, non-toxicity and resistance against corrosion [15-19]. In practical applications however, ZnO has narrow range of spectral response especially under UV irradiation ($\lambda < 380 \text{ nm}$) which contributes to only 6-8% of solar energy whereas visible light contributes 46%. Further, due to less separation between the photo-generated charge carriers, recombination and dissipation of energy takes place in nanoseconds, making it difficult to utilize the photo-generated electrons and holes. These electrons and holes act as powerful oxidizing and reducing agents respectively

and a delayed recombination can make them suitable for redox reactions, which leads to better photocatalysis [20, 21]. Hence to obtain a better photocatalyst out of ZnO, its absorption edge needs to be shifted towards the visible region and photogenerated electrons and holes need to have a better charge separation. These requirements can be achieved by doping rare earth ions into the ZnO matrix [22-26]. Monovalent doping of lanthanides *viz.* lanthanum (La), cerium (Ce), dysprosium (Dy) has been extensively studied [27-31]. Amongst these monovalent rare earth dopants, cerium is distinctly interesting due to its large ionic radius, which causes a localized charge perturbation when substituted into the lattice of ZnO and hence leads to better photocatalysis [32-36]. Few precedents of divalent dopings are available in the literature, showing such doping leads to much better and improved photocatalysis and bandgap tailoring [37-43]. There are no studies on trivalent doping of ZnO in literature. This motivated us to do a detailed analysis of Lanthanum, Cerium and dysprosium co-doping into ZnO matrix and we observed much improved optical properties. The improvement was observed on multiple fronts. We hereby report a facile and cost effective synthesis of La, Ce, Dy co-doped ZnO nanoparticles with improved and optimized photocatalytic activities, a better dopant dependent bandgap, red shift in the absorption edge and much improved charge separation between the photogenerated charge carriers. Better charge separation is a consequence of dopant induced trap levels in the bandgap of ZnO.

Several methods have been utilized so far for the synthesis of rare earth doped ZnO nanoparticles which include forced hydrolysis [44], pulsed laser deposition [45] and combustion methods [46]. All these methods are quite complex and require costly machinery, high temperatures and toxic chemicals.

In the present work, we report a facile, cost effective and environmental friendly co-precipitation technique for synthesizing La, Ce, Dy co-doped ZnO nanoparticles with varying stoichiometry *viz.* $\text{Zn}_{0.97}\text{La}_{0.01}\text{Ce}_{0.01}\text{Dy}_{0.01}\text{O}$, $\text{Zn}_{0.94}\text{La}_{0.02}\text{Ce}_{0.02}\text{Dy}_{0.02}\text{O}$, $\text{Zn}_{0.91}\text{La}_{0.03}\text{Ce}_{0.03}\text{Dy}_{0.03}\text{O}$, $\text{Zn}_{0.88}\text{La}_{0.04}\text{Ce}_{0.04}\text{Dy}_{0.04}\text{O}$ and $\text{Zn}_{0.85}\text{La}_{0.05}\text{Ce}_{0.05}\text{Dy}_{0.05}\text{O}$. Optical properties of all dopant concentrations were compared. Structural, morphological, photoluminescence and bandgap studies were done using XRD, SEM, PL and DRS respectively. Photocatalytic properties of undoped La, Ce, Dy doped ZnO nanoparticles were analyzed by observing the decomposition of Rhodamine B under UV light irradiation. The degradation of harmful dye and ensuing removal of color was much improved in La, Ce, Dy co-doped samples as compared to the undoped ZnO. The detailed mechanism of photocatalytic degradation of Rhodamine B dye is discussed in the present work.

2. Experimental Procedure.

A low cost, facile and environment friendly co-precipitation approach was utilized for synthesizing La, Ce, Dy co-doped ZnO nanoparticles ($\text{Zn}_{0.97}\text{La}_{0.01}\text{Ce}_{0.01}\text{Dy}_{0.01}\text{O}$, $\text{Zn}_{0.94}\text{La}_{0.02}\text{Ce}_{0.02}\text{Dy}_{0.02}\text{O}$, $\text{Zn}_{0.91}\text{La}_{0.03}\text{Ce}_{0.03}\text{Dy}_{0.03}\text{O}$, $\text{Zn}_{0.88}\text{La}_{0.04}\text{Ce}_{0.04}\text{Dy}_{0.04}\text{O}$ and $\text{Zn}_{0.85}\text{La}_{0.05}\text{Ce}_{0.05}\text{Dy}_{0.05}\text{O}$). The mole fraction of the constituent ions was maintained by controlling the weight ratio of dopants La, Ce and Dy to host Zn. The starting material and the dopant sources used *viz.* zinc acetate dihydrate [$\text{Zn}(\text{COOCH}_3)_2 \cdot 2(\text{H}_2\text{O})$], lanthanum(III)acetate sesquihydrate [$\text{La}(\text{CH}_3\text{COO})_3 \cdot 1.5(\text{H}_2\text{O})$], Cerium(III)acetate tetrahydrate [$\text{Ce}(\text{CH}_3\text{COO})_3 \cdot 4\text{H}_2\text{O}$] and dysprosium(III)acetate tetrahydrate [$\text{Dy}(\text{CH}_3\text{COO})_3 \cdot 4\text{H}_2\text{O}$], were of high purity (Sigma Aldrich 99% purity) and were used as such without any further purification. Distilled water was used as the reaction medium and diethylamine as the reducing as well as stabilizing agent. To begin with, undoped ZnO nanoparticles were synthesized by taking 0.5 M zinc acetate solution

in a beaker at 60 °C and adding 5 ml of diethylamine slowly to it. The solution was stirred at 60 °C for 30 mins followed by heating at 180 °C. The resulting powders were obtained by centrifugation and were annealed at 500 °C in a muffle furnace for 1hour.

In order to obtain the La, Ce, Dy co-doped samples i.e. $\text{Zn}_{0.97}\text{La}_{0.01}\text{Ce}_{0.01}\text{Dy}_{0.01}\text{O}$, $\text{Zn}_{0.94}\text{La}_{0.02}\text{Ce}_{0.02}\text{Dy}_{0.02}\text{O}$, $\text{Zn}_{0.91}\text{La}_{0.03}\text{Ce}_{0.03}\text{Dy}_{0.03}\text{O}$, $\text{Zn}_{0.88}\text{La}_{0.04}\text{Ce}_{0.04}\text{Dy}_{0.04}\text{O}$ and $\text{Zn}_{0.85}\text{La}_{0.05}\text{Ce}_{0.05}\text{Dy}_{0.05}\text{O}$, the dopant ion salts were used to prepare their solutions in distilled water with concentrations varying from 0.01 M to 0.05 M. These solutions were then added to 0.5 M ZnO solution under stirring at 60 °C. 5 ml of diethylamine was added to this solution dropwise. The heating was further continued for 1hour and the resulting powders were centrifuged and cleaned with ethanol and annealed at 500 °C for each molar concentration from 0.01M to 0.05M. The standard conditions and molarities for the synthesis of La, Ce, Dy co-doped ZnO nanoparticles are depicted in table 1.

The structural properties of nanoparticles were examined using X- Ray diffractometer with CuK α target ($k = 1.54052 \text{ \AA}$). The radiation was over the range of 2θ from 10–90° and step was 0.01. The morphological features of undoped ZnO and La, Ce, Dy co-doped ZnO nanoparticles was observed under SEM. Horiba LabRam spectrometer with an excitation source of 325 nm (wavelength) and an accumulation time of 2 seconds was used to record the PL spectrum of the undoped and doped ZnO nanoparticles. Optical studies were done using DRS, UV-Vis,- NIR spectrometer at a normal incidence of powder samples (USB 2000 and deuterium halogen power source DH-2000 Micropack; Ocean Optics).

2.1. Photocatalytic Activity measurement.

To measure the photocatalytic activity of undoped and La, Ce, Dy co-doped ZnO nanoparticles, 40 mg of nanoparticle powder was weighed. In a 250 ml beaker 10 ml of 10 ppm Rhodamine B dye solution was taken and to this 30 ml of distilled water was added. Finally the weighed nanoparticle powder was added to this dye solution. This solution was wrapped, kept in dark and stirred for half an hour to disperse the photocatalyst nanoparticles and establish adsorption-desorption equilibrium. Afterwards the solution was irradiated with UV light in the photocatalytic reactor (M/S Technistro, Nagpur, Maharashtra) fitted with high pressure mercury lamp with capacity 450 W (operating voltage, 110-220 V), whilst the stirring was continued. A 3 ml aliquot was taken at an interval of 10 mins and immediately centrifuged to remove nanocatalyst. Absorbance of the samples was measured using UV-Vis spectrometer (Perkin Elmer lambda 35) run between 400-600 nm. A decrease in absorbance and removal of dye color confirmed the degradation of Rhodamine B dye with undoped and La, Ce, Dy co-doped ZnO as photocatalyst.

3. Results and Discussion

3.1. Structural Analysis.

Fig.1 (a) reveals the XRD pattern of undoped and La, Ce, Dy co-doped ZnO nanoparticles with concentrations ($\text{Zn}_{0.97}\text{La}_{0.01}\text{Ce}_{0.01}\text{Dy}_{0.01}\text{O}$, $\text{Zn}_{0.94}\text{La}_{0.02}\text{Ce}_{0.02}\text{Dy}_{0.02}\text{O}$, $\text{Zn}_{0.91}\text{La}_{0.03}\text{Ce}_{0.03}\text{Dy}_{0.03}\text{O}$, $\text{Zn}_{0.88}\text{La}_{0.04}\text{Ce}_{0.04}\text{Dy}_{0.04}\text{O}$ and $\text{Zn}_{0.85}\text{La}_{0.05}\text{Ce}_{0.05}\text{Dy}_{0.05}\text{O}$) ZnO nanoparticles XRD analysis shows all the nanoparticles formed are of hexagonal wurtzite phase as per the The International Centre for Diffraction Data (ICDD) database number 01-070-8072. The broadness of all the peaks indicated purely crystalline nature of the nanoparticles. Further analysis revealed there were no secondary peaks other than ZnO indicating all the samples formed were pure phase. The ionic radius of host ion Zn^{2+} (0.72 Å) is small as compared to the dopant ions i.e. La^{3+} (1.06 Å), Ce^{3+}

(1.03 Å) and Dy³⁺ (0.91 Å) which leads to distortion in the ZnO lattice and also there is a shift towards lower angle in the doped samples, confirming substitutional doping of La, Ce, Dy co-dopants in ZnO matrix which is shown in **Fig. 1(b)**. The formulae used for the calculation of lattice parameters and crystallite size respectively are listed below and the numeric values of same are given in table 2. Mismatch of ionic radii of host Zn²⁺ ion and dopant ions leads to an increase in bond length which gets reflected in increased values of lattice constants *a* and *c* as shown in table 2.

$$a = \frac{\lambda}{\sqrt[3]{\sin\theta}} \quad (1)$$

$$b = \frac{\lambda}{\sin\theta} \quad (2)$$

$$D = \frac{K\lambda}{\beta \cos\theta} \quad (3)$$

In the above formulae λ represents the wavelength of target used in the X-ray diffractometer used and its value is 1.5406 Å. θ and *K* represent the diffraction angle and the shape factor respectively, *D* is crystallite size and β denotes full width half maximum. The crystallite size decreases from 47 nm in case of undoped ZnO to around 35 nm in case of doped nanoparticles, hence dopant concentration restricts the growth of nanoparticles in doped samples and which was confirmed and explained using scanning electron microscopy SEM.

3.2. Morphological Studies.

The SEM micrographs of undoped and La, Ce, Dy co-doped ZnO with concentrations Zn_{0.97}La_{0.01}Ce_{0.01}Dy_{0.01}O, Zn_{0.94}La_{0.02}Ce_{0.02}Dy_{0.02}O, Zn_{0.91}La_{0.03}Ce_{0.03}Dy_{0.03}O, Zn_{0.88}La_{0.04}Ce_{0.04}Dy_{0.04}O and Zn_{0.85}La_{0.05}Ce_{0.05}Dy_{0.05}O, are shown in **Fig.2 (a-e)**. It can be clearly seen from the SEM micrographs that the SEM results are in concurrence with the XRD results. Increase in dopant concentration leads to decrease in particle size. Ionic radii of dopant ions La³⁺

(1.06 Å), Ce^{3+} (1.03 Å) and Dy^{3+} (0.91 Å) are quite large as compared to the host Zn^{2+} ion i.e. (0.72 Å). This mismatch in ionic radii leads to lattice strain and eventually a decreased grain size in case of doped nanoparticles. It can be observed from the SEM micrographs that on increasing the dopant concentration the morphology of the nanoparticles eventually becomes flower like. This phenomenon can be credited to the Ce^{3+} ion doping which plays a pivotal role in capping the nanoparticles formed after nucleation [47]. The Ce^{3+} ions cause steric hindrances in presence of a strongly absorbed reducing agent- diethylamine, which leads to formation of flower like structure in case of La, Ce, Dy co-doped ZnO nanoparticles. This can be further explained with the help of growth and nucleation of nanoparticles. A precursor initiates the formation of seed nuclei which then grow to form rods by Ostwald ripening effect, in which larger particles grow at the expense of smaller particles. Solvent facilitates this process and various subunits formed are connected by the orientation attachment process leading to flower like morphology [48].

3.3. Photoluminescence Studies.

Important properties of semiconductors like bandgap, energy levels, chemical composition and type of impurity can be extensively studied with the help of photoluminescence (PL). The PL spectra of undoped and La, Ce, Dy co-doped ZnO nanoparticles are shown in **Fig. 3(a)**. The spectra were obtained by exciting the sample at a wavelength of 325 nm. The PL spectrum of pure or undoped ZnO depicts two prominent emission peaks at 390 nm and 710 nm. The first prominent peak at 390 nm corresponds to the UV region and can be due to near band edge emission caused by the recombination of free and bound exciton pairs. The second peak at 710 nm corresponds to the near infrared region and is possibly ascribed to surface plasma resonance [49]. It is clear from **Fig.3 (a)** La, Ce, Dy co-doping has two important influences on the

photoluminescence emission peaks in UV region that is decrease in intensity of emission peaks and shifting of emission peaks towards the higher wavelength. Decrease in intensity can be attributed to the transfer of energy from host ZnO to dopants La, Ce and Dy which confirms perfect substitution of dopants into the host matrix. Decrease in peak intensity and consequent decrease in energy also indicates delayed recombination with increase in dopant concentration. This pertains to the fact that increased dopant concentration leads to surface bound states acting as trap states resulting in non radiative relaxation. The PL intensity depends on the distance between these trap states and their centre to centre interaction. The spectral overlap between the wave functions of these states leads to dissipation of energy in non-radiative manner and consequent decrease in energy [50]. La, Ce, Dy co-doping also leads to shifting of the peak in UV region towards the visible region of spectrum as can be seen in **Fig. 3(b)**. This is a very important consequence which can lead to better utilization of the solar energy and pave way for excellent optoelectronic applications. This red shift can be attributed to creation of electronic states near the conduction band of ZnO due to presence of dopants, which also leads to narrowing of bandgap of ZnO as has already been reported in Ce-doped nitrides [51]. Narrowing of bandgap can further be credited to the narrow optical transitions within spin orbital levels due to tailoring of conduction and valence bands caused by dopant induced potential fluctuations [52]. As the electronegativities of the dopant ions La^{3+} (1.1), Dy^{3+} (1.22) and Ce^{3+} (1.12) are less than the electronegativity of host Zn^{2+} (1.65), the columbic interaction between electrons-holes pairs bound by isoelectronic levels formed by La, Ce and Dy generates acceptor bound excitation pair. This leads to charge transfer between conduction band of ZnO and different states of dopants, effecting a red shift which consequently narrows the bandgap.

3.4. Photocatalytic studies.

The photocatalytic activities of undoped and La, Ce, Dy co-doped ZnO nanoparticles were evaluated by observing the degradation of Rhodamine B dye under UV light irradiation and using these nanoparticles as photocatalysts. **Fig. 4 (a-f)** reveals the degradation of Rhodamine B dye with ZnO and La, Ce, Dy co-doped ZnO as nano photocatalysts within reaction times from 0-60 min. Degradation is confirmed as the absorbance of dye decreases with increase in concentration of dopants and reaction time. We observed the fastest and most efficient degradation with $\text{Zn}_{0.85}\text{La}_{0.05}\text{Ce}_{0.05}\text{Dy}_{0.05}\text{O}$ nanoparticles as photocatalyst. The photocatalytic performance of undoped and La, Ce, Dy co- doped ZnO nanaoprticles was evaluated by taking the plot between C_t/C_o and irradiation time (t), where C_o is the initial dye concentration and C_t is the residual dye concentration after a time interval t as shown in **Fig. 5(a)**. Degradation of Rhodamine B dye roughly obeys pseudo first order kinetics for low concentration of dyes [54].

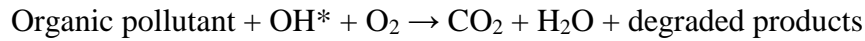
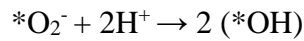
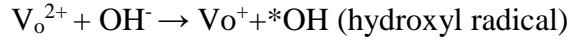
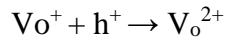
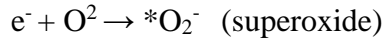
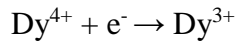
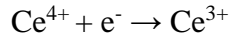
$$\ln[C_t/C_o] = K * t \quad (4)$$

Where K represents the constant-kinetic parameter and is different for different photocatalysts. The value of constant K can be found by linear fitting the slope of graph obtained between $\ln(C_t/C_o)$ and irradiation time t as is shown in **Fig.5 (b)**. The values of K obtained in this case were 0.0247 S^{-1} , 0.0408 S^{-1} , 0.0407 S^{-1} , 0.055 S^{-1} , 0.058 S^{-1} and 0.060 S^{-1} for undoped and La, Ce, Dy co-doped ZnO nanoparticles ($\text{Zn}_{0.97}\text{La}_{0.01}\text{Ce}_{0.01}\text{Dy}_{0.01}\text{O}$, $\text{Zn}_{0.94}\text{La}_{0.02}\text{Ce}_{0.02}\text{Dy}_{0.02}\text{O}$, $\text{Zn}_{0.91}\text{La}_{0.03}\text{Ce}_{0.03}\text{Dy}_{0.03}\text{O}$, $\text{Zn}_{0.88}\text{La}_{0.04}\text{Ce}_{0.04}\text{Dy}_{0.04}\text{O}$ and $\text{Zn}_{0.85}\text{La}_{0.05}\text{Ce}_{0.05}\text{Dy}_{0.05}\text{O}$) respectively. The value of K was found to be highest in case of highest doping concentration i.e. $\text{Zn}_{0.85}\text{La}_{0.05}\text{Ce}_{0.05}\text{Dy}_{0.05}\text{O}$. The degradation efficiency was further studies by calculating the degradation percentage using the formula given below.

$$\%D = \left(1 - C_t/C_o\right) * 100 \quad (5)$$

Where % D is the degradation percentage, C_o is the initial concentration of dye and C_t is the concentration of dye after interval t . Degradation percentage was found to be highest (93%) for $\text{Zn}_{0.85}\text{La}_{0.05}\text{Ce}_{0.05}\text{Dy}_{0.05}\text{O}$ nanoparticles as photocatalyst. This is depicted graphically in **Fig. 5(c)**. Enhanced photocatalytic activity of ZnO nanoparticles with trivalent rare earth doping can be explained by investigating the degradation mechanism of Rhodamine B dye as follows. The semiconductor nanoparticles to be investigated as photocatalysts are initially excited with photons having energy greater than the bandgap i.e. ($h\nu > \text{bandgap}$). This excitation generates electron hole pairs on the surface of the nanoparticle. These photo-generated electron hole pairs are trapped by oxygen (O_2), which is adsorbed on the surface of the nanoparticle. This trapping of photo-generated electrons and holes is the rate determining step in photocatalysis reaction. The $4f$ configuration of rare earth dopants also plays a pivotal role in generation, delayed recombination and delayed charge transfer of electron hole pairs. La^{4+} , Ce^{4+} and Dy^{4+} act as scavenger for the electron from conduction band as these are stronger Lewis acids compared to O_2 and hence better at trapping the electrons and holes. The electrons trapped by the dopants are transferred oxidatively to the surface adsorbed oxygen to produce the superoxide radical ($^*\text{O}_2^-$). The electrons and holes generated by high energy photons can easily recombine and dissipate the energy, which prevents their efficient utilization. The recombination of photo-generated electrons and holes can be prevented in the presence of defect states. In the present work, singly oxygen vacancies (Vo^+) act as trap states to enhance the separation between photo-generated electrons and holes. The singly oxygen vacancy acts as electron donor to become charged oxygen vacancy which then acts as trap for photo-generated holes and prevents recombination. This charged oxygen vacancy on reaction with the hydroxyl ion (OH^-) forms hydroxyl radical (OH^*). This can be summarized as,

Incident photons + ZnO \rightarrow electrons (e^-) + holes (h^+)



Oxygen vacancies don't only trap holes, they also help in adsorbing oxygen and hence further enhance photocatalysis [55].

The efficiency of any photocatalyst depends on a number of factors which include number of charge carriers on the surface, and recombination rate of the electron hole pairs generated upon incidence of high energy photon. In the present work, rare earth doping in ZnO has been utilized to increase its photocatalytic activity many folds as compared to the undoped ZnO. The reason for this can be credited to loading of charge carriers on the surface as a consequence of decrease in size and increase in surface area on doping and presence of oxygen vacancies in the bandgap of ZnO due to trivalent rare earth doping. Photoluminescence (PL) studies **Fig. 3 (a-b)** reveal that the trivalent rare earth doping causes the shifting of absorption edge towards the visible region and narrowing of bandgap. Both these effects can lead to better utilization of solar energy and hence more efficient photocatalysis. Further PL spectrum reveals incorporation of additional levels in the bandgap of ZnO upon rare earth doping which further delays the recombination of charge carriers leading to efficient photocatalysis. This red shift in absorption edge and bandgap narrowing are also confirmed by diffuse reflectance studies (DRS).

3.5. Optical Studies, Diffuse Reflectance Studies-(DRS).

Fig.6 (a) depicts the diffuse reflectance spectra of undoped and La, Ce, Dy co-doped ZnO nanoparticles of following concentrations ($\text{Zn}_{0.97}\text{La}_{0.01}\text{Ce}_{0.01}\text{Dy}_{0.01}\text{O}$, $\text{Zn}_{0.91}\text{La}_{0.03}\text{Ce}_{0.03}\text{Dy}_{0.03}\text{O}$, and $\text{Zn}_{0.85}\text{La}_{0.05}\text{Ce}_{0.05}\text{Dy}_{0.05}\text{O}$). All the samples showed high reflection in visible region, confirming a small absorption of visible light by all samples. Co-doping was seen to enhance the percentage of visible light reflectance, which has also been reported previously [56, 57]. The bandgap was calculated from the reflectance using the Kubela-Munk function:

$$F(R) = (1 - R)^2 / 2R \quad (6)$$

Where $F(R)$ the Kubela-Munk is function and R represents the reflectance [58, 59], R is found from the y axis of the plot between reflectance and wavelength **Fig. 6 (a)**. $F(R)$ is calculated using the above formula and then a plot is drawn between $[F(R)hv]^2$ vs hv . Here h is the Plank's constant and ν is the frequency, $\nu = 1/\lambda$ and wavelength λ is found from x -axis of graph shown in **Fig. 6 (a)**. The lines in **Fig. 6 (b)** show the extrapolation of linear portion of plot $F(R)hv]^2$ vs hv . The points at which these lines touch the x -axis give us the bandgap values. The bandgap of undoped ZnO was found to be 3.12 eV. For doped samples a decrease in bandgap was observed. Band gap values of 3.04 eV, 3.0 eV and 2.85 eV were found for $\text{Zn}_{0.97}\text{La}_{0.01}\text{Ce}_{0.01}\text{Dy}_{0.01}\text{O}$, $\text{Zn}_{0.91}\text{La}_{0.03}\text{Ce}_{0.03}\text{Dy}_{0.03}\text{O}$, and $\text{Zn}_{0.85}\text{La}_{0.05}\text{Ce}_{0.05}\text{Dy}_{0.05}\text{O}$ samples respectively. Red shift along with narrowing of bandgap can be attributed to the creation of additional trap or defect states in the bandgap of ZnO and formation of oxygen vacancies due to doping. These lead to increase in average atomic distance and hence decrease in bandgap.

4. Conclusion.

Pure and La, Ce, Dy co-doped ZnO nanoparticles were successfully prepared using a facile and cost effective approach of co-precipitation. Successful formation of nanoparticles was confirmed

by XRD. A slight distortion in XRD pattern of doped samples was found due to ionic radii mismatch between host and dopant ions. Average particle size was found to be around 35 nm. Morphology was evaluated using SEM, and the doped nanoparticles were found to have a flower like morphology. Photoluminescence PL studies revealed a red shift in absorption edge and narrowing of bandgap. Tunable band gap makes the doped nanoparticles excellent candidates for optoelectronic applications. Photocatalytic studies confirmed an enhanced and optimized photocatalytic performance in case of La, Ce, Dy co-doped samples due to delayed recombination of photogenerated charge carriers, creation of additional levels in the band gap of ZnO, increased surface oxygen vacancies and charge transfer. The sample, $\text{Zn}_{0.85}\text{La}_{0.05}\text{Ce}_{0.05}\text{Dy}_{0.05}\text{O}$ exhibited the best photo-catalytic performance for the degradation of Rhodamine B dye.

References:

- [1]. P. Thiagarajan, M. Kottaisamy, K. Sethupathi and M. S. R. Rao, J. Displays, **30**, 202, (2009).
- [2]. C. Zhang and J. Lin, Chem. Soc. Rev., **41**, 7938, (2012).
- [3]. M. Shang, G. Li, D. Yang, X. Kang, C. Peng, Z. Cheng and J. Lin, Dalton Trans., **40**, 9379, (2011).
- [4]. P. V. Korake, R. S. Dhabbe, A. N. Kadam, Y. B. Gaikwad and K. M. Garadkar, J. Photochem. Photobiol. B, **130**, 11, (2014).
- [5]. Ü. Özgür, Y. I. Alivov, C. Liu, A. Teke, M. A. Reshchikov, S. Doğan, V. Avrutin, S. J. Cho and H. Morkoç, J. Appl. Phys., **98**, 041301, (2005).
- [6]. U. O. H. Morkoc, Zinc Oxide: Fundamentals, Materials and Device Technology, Wiley, (2009).

- [7]. S. Baskoutas and G. Bester, J. Phys. Chem. C, **114**, 9301, (2010).
- [8]. S. C. Erwin, L. Zu, M. I. Haftel, A. L. Efros, T. A. Kennedy and D. J. Norris, Nature,**436**, 91, (2005).
- [9]. D. J. Norris, A. L. Efros and S. C. Erwin, Science, **319**, 1776, (2008).
- [10]. K. Yim, J. Lee, D. Lee, M. Lee, E. Cho, H. S. Lee, H.-H. Nahm and S. Han, Sci. Rep., **7**, 40907, (2017).
- [11]. T. Makino, Y. Segawa, S. Yoshida, A. Tsukazaki, A. Ohtomo and M. Kawasaki, Appl. Phys. Lett., **85**, 759, (2008).
- [12]. S. Singh, N. Rama and M. S. R. Rao, Appl. Phys. Lett., **88**, 222111, (2006).
- [13]. A. Azarov, A. Galeckas, A. Hallén, A. Kuznetsov, E. Monakhov and B. G. Svensson, J. Appl. Phys., **118**, 125703, (2015).
- [14]. A. Kunz, P. Peralta-Zamora, S. G. de Moraes, N. Duran, Quimica Nova, **25**, 78, (2002).
- [15]. P. V. Korake, A. N. Kadam, K. M. Garadkar, J. Rare Earths, **32**, 306, (2014).
- [16]. N. Shaari, S. H. Tan, A. R. Mohamed, J. Rare Earths, **30**, 651, (2012.)
- [17]. X. J. Yu, L. L. Xiong, G. P. Ma, Y. Liang, K. R. Liu., J. Rare Earths, **32**,849, (2014).
- [18]. C. Wang, L .Cao, J. Rare Earths, **29**, 727, (2011).
- [19]. J. Wu, G. L. Zhang, J. Liu, H. B. Gao, C. X. Song, H.R Du, Z. Li, Z.P Gong, Y.G Lu. J. Rare Earths, **32**, 727, (2014).
- [20]. A. L. Linsebigler, G. Q. Lu, J.T. Yates Jr., Chem. Rev., **95**, 735, (1995).

- [21]. M. Romero, J. Blanco, B. Sanchez, A. Vidal, S. Malato, A. I. Cardona *et. al.*, Sol. Energy, **66**, 169, (1999).
- [22]. M. Ahmad, E. Ahmed , Z. L. Hong , J. F Xu, N. R. Khalid, A. Elhissi, W. Ahmed, J. Alloys Compd., **577**, 717, (2013).
- [23]. M. Ahmad, E. Ahmed, Z. L. Hong, Z. Iqbal, N. R. Khalid, T. Abbas, I. Ahmad, A. Elhissi, W. Ahmed, Ceram. Int., **39**, 8693, (2013).
- [24]. M. Ahmad, E. Ahmed, Z. L. Hong, X. L. Jiao, T. Abbas, N. R. Khalid, Appl. Surf. Sci., **285P**, 702, (2013).
- [25]. H. S. Cai, G. G. Liu, W. Y. Lu, X. X. Li, L. Yu, D. G. Li, J. Rare Earths, **26**, 71, (2008).
- [26]. S. Kumar, P. D. Sahare, J. Rare Earths, **30**, 761, (2012).
- [27]. D. K. Sharma, K. K. Sharma, V. Kumar and A. Sharma, J. Mater. Sci.: Mater. Electron., **27**, 10330, (2016).
- [28]. Q. Shi, C. Wang, S. Li, Q. Wang, B. Zhang, W. Wang, J. Zhang and H. Zhu, Nanoscale Res. Lett., **9**, 480, (2014).
- [29]. M. Ahmad, E. Ahmed, F. Zafar, N. R. Khalid, N. A. Niaz, A. Hafeez, M. Ikram, M. A. Khan and Z. Hong, J. Rare Earths, **33**, 255, (2015).
- [30]. N. C. S. Selvam, J. J. Vijaya and L. J. Kennedy, J. Nanosci. Nanotechnol, **13**, 1, (2013).
- [31]. S. Rajendran, M. M. Khan, F. Gracia, J. Qin, V. K. Gupta and S. Arumainathan, Sci. Rep., **6**, 31641, (2016).
- [32]. H. X. Shi, T. Y. Zhang, H.L. Wang. J. Rare Earths, **29**, 746, (2011).
- [33]. R. Zeng, J. G. Wang, J. Y. Cui, L. Hu, K.G. Mu, J. Rare Earths, **28**, 353, (2010).
- [34]. C. M. Fan, P. Xue, Y.P. Sun, J. Rare Earths, **24**, 309, (2006).

- [35]. L. Bian, M. X. Song, T. L. Zhou, X. Y. Zhou, Q. Q. Dai. J. Rare Earths, **27**, 461, (2009).
- [36]. M. Zalaj, J. Rare Earths, **32**, 487, (2014).
- [37]. R. K. Kalaiezhily, V. Asvini, G. Saravanan and K. Ravichandran, Dalton Trans., **48**, 12228, (2019).
- [38]. J. Iqbal, X. Liu , H. Zhu, Z.B. Wua, Y. Zhang, D. Yu, R. Yu, Acta Mater., **57**, 4790, (2009).
- [39]. P. Pascariu, M. Homocianu, C. Cojocaru, P. Samoila, A. Airinei, M. Sucheai, Appl. Surf. Sci., **476**, 16, (2019).
- [40]. M. Romero, J. Blanco, B. Sanchez, A. Vidal, S. Malato, A. I. Cardona *et. al.*, Sol. Energy, **66**,169, (1999).
- [41]. A. Rahman, R. Jayaganthan, Trans. Indian Inst. Met., **70**, 1063, (2016).
- [42]. C. A. Arguello, D. L. Rousseau, S. P. S. Porto, Phys. Rev., **181**, 351, (1969).
- [43]. R. Bomila, S. Suresh, S. Srinivasan, J. Mater. Sci: Mater. Electron., **30**, 582, (2019).
- [44]. X. Z. Li, F. B. Li, C. L. Yang, W. K. Ge, J. Photochem. Photobiol. A, **141**, 209, (2009).
- [45]. L. Q. Jing, X. J. Sun, W. M. Cai, Z. L. Xu, Y. G. Du, H. G. Fu, J. Phys. Chem. Solid, **64**, 615, (2003).
- [46]. H. Yamashita, Y. Ichihashi, S. G. Zhang, Y. Matsumurab, Y. Soumab, T. Tatsumic, *et al.* Appl. Surf. Sci., **121**, 305311, (1997).
- [47]. R. Bomila, S. Srinivasan, A. Venkatesan, B. Bharath,K. Perinbam, Mater. Res. Innov., **22**, 379, (2017).
- [48]. X. Liu, D. G. Sroppa, M. Heggan, Y. Ermolenko , A. Offenhausser, Y. Mourzina, J. Phys. Chem. C, **119**, 10336, (2015).
- [49]. J. H. Zeng, Y. L. Yu, Y. F. Wang, T. Lou, J. Acta. Mater., **57**, 1813, (2009).

- [50]. A. George, S. K. Sharma, S. Chawla, M. M. Malik, M. S. Qureshi, J. alloys. Compd., **509**, 5942, (2011).
- [51]. A. Majid, A. Ali, J. Phys. D: Appl. Phys., **42**, 45412, (2009).
- [52]. K. F. Berggren, B. E. Sernelius, Phys. Rev., **24**, 1971, (1981).
- [53]. S. Bhatia, N. Verma, Mater. Res. Bull., **95**, 468, (2017).
- [54]. S. Wang, L. Bai, X. Ao, RSC Adv., **8**, 36745, (2018).
- [55]. C. J. Chang, C. Y. Lin, M. H. Hsu, J. Taiwan. Inst. Chem. Eng., **45**, 1954, (2014).
- [56]. R. K. Kalaiezhily, G. Saravanan, V. Asvini, N. Vijayan and K. Ravichandran, Ceram. Int., **44**, 19560, (2018).
- [57]. R. K. Kalaiezhily, V. Asvini, G. Saravanan and K. Ravichandran, J. Mater. Sci.: Mater. Electron., **29**, 12001, (2018).
- [58]. R. López and R. Gómez, J. Sol-Gel Sci. Technol., **61**, 1, (2012).
- [59]. P. Kubelka, J. Opt. Soc. Am., **38**, 448, (1948).

List of Figures and Table captions

- 1) **Figure 1(a, b)** (a) XRD pattern of un-doped ZnO and La, Ce, Dy co-doped ZnO nanoparticles ($\text{Zn}_{0.97}\text{La}_{0.01}\text{Ce}_{0.01}\text{Dy}_{0.01}\text{O}$, $\text{Zn}_{0.94}\text{La}_{0.02}\text{Ce}_{0.02}\text{Dy}_{0.02}\text{O}$, $\text{Zn}_{0.91}\text{La}_{0.03}\text{Ce}_{0.03}\text{Dy}_{0.03}\text{O}$, $\text{Zn}_{0.88}\text{La}_{0.04}\text{Ce}_{0.04}\text{Dy}_{0.04}\text{O}$ & $\text{Zn}_{0.85}\text{La}_{0.05}\text{Ce}_{0.05}\text{Dy}_{0.05}\text{O}$) (b) Expanded XRD pattern showing shift towards lower angle with increase in co-dopant concentration.
- 2) **Figure 2(a-f)** SEM surface micrographs of un-doped ZnO and La, Ce, Dy co-doped ZnO nanoparticles. (a) Un-doped ZnO, (b) $\text{Zn}_{0.97}\text{La}_{0.01}\text{Ce}_{0.01}\text{Dy}_{0.01}\text{O}$, (c) $\text{Zn}_{0.94}\text{La}_{0.02}\text{Ce}_{0.02}\text{Dy}_{0.02}\text{O}$, (d) $\text{Zn}_{0.91}\text{La}_{0.03}\text{Ce}_{0.03}\text{Dy}_{0.03}\text{O}$, (e) $\text{Zn}_{0.88}\text{La}_{0.04}\text{Ce}_{0.04}\text{Dy}_{0.04}\text{O}$ (f) $\text{Zn}_{0.85}\text{La}_{0.05}\text{Ce}_{0.05}\text{Dy}_{0.05}\text{O}$.
- 3) **Figure 3(a, b)** (a) Room temperature PL spectrum of un-doped and La,Ce,Dy co-doped ZnO nanoparticles ($\text{Zn}_{0.97}\text{La}_{0.01}\text{Ce}_{0.01}\text{Dy}_{0.01}\text{O}$, $\text{Zn}_{0.94}\text{La}_{0.02}\text{Ce}_{0.02}\text{Dy}_{0.02}\text{O}$, $\text{Zn}_{0.91}\text{La}_{0.03}\text{Ce}_{0.03}\text{Dy}_{0.03}\text{O}$, $\text{Zn}_{0.88}\text{La}_{0.04}\text{Ce}_{0.04}\text{Dy}_{0.04}\text{O}$ & $\text{Zn}_{0.85}\text{La}_{0.05}\text{Ce}_{0.05}\text{Dy}_{0.05}\text{O}$) (b)

Expanded UV region of the spectrum showing red shift in wavelength with increase in concentration of dopants.

- 4) **Figure 4(a-e)** UV-Vis Absorbance spectral changes of Rhodamine B dye solution during photocatalytic degradation with undoped and La, Ce, Dy co-doped ZnO nanoparticles under UV irradiation at different time intervals. (a) Un-doped ZnO, (b) $\text{Zn}_{0.97}\text{La}_{0.01}\text{Ce}_{0.01}\text{Dy}_{0.01}\text{O}$, (c) $\text{Zn}_{0.94}\text{La}_{0.02}\text{Ce}_{0.02}\text{Dy}_{0.02}\text{O}$, (d) $\text{Zn}_{0.91}\text{La}_{0.03}\text{Ce}_{0.03}\text{Dy}_{0.03}\text{O}$, (e) $\text{Zn}_{0.88}\text{La}_{0.04}\text{Ce}_{0.04}\text{Dy}_{0.04}\text{O}$ & (f) $\text{Zn}_{0.85}\text{La}_{0.05}\text{Ce}_{0.05}\text{Dy}_{0.05}\text{O}$.
- 5) **Figure 5 (a-c)** (a) Photocatalytic degradation of Rhodamine B dye solution un-doped and La, Ce, Dy co-doped ZnO nanoparticles ($\text{Zn}_{0.97}\text{La}_{0.01}\text{Ce}_{0.01}\text{Dy}_{0.01}\text{O}$, $\text{Zn}_{0.94}\text{La}_{0.02}\text{Ce}_{0.02}\text{Dy}_{0.02}\text{O}$, $\text{Zn}_{0.91}\text{La}_{0.03}\text{Ce}_{0.03}\text{Dy}_{0.03}\text{O}$, $\text{Zn}_{0.88}\text{La}_{0.04}\text{Ce}_{0.04}\text{Dy}_{0.04}\text{O}$ & $\text{Zn}_{0.85}\text{La}_{0.05}\text{Ce}_{0.05}\text{Dy}_{0.05}\text{O}$) (b) Reaction kinetics of photocatalytic degradation with un-doped ZnO nanoparticles and La, Ce, Dy co-doped ZnO nanoparticles ($\text{Zn}_{0.97}\text{La}_{0.01}\text{Ce}_{0.01}\text{Dy}_{0.01}\text{O}$, $\text{Zn}_{0.94}\text{La}_{0.02}\text{Ce}_{0.02}\text{Dy}_{0.02}\text{O}$, $\text{Zn}_{0.91}\text{La}_{0.03}\text{Ce}_{0.03}\text{Dy}_{0.03}\text{O}$, $\text{Zn}_{0.88}\text{La}_{0.04}\text{Ce}_{0.04}\text{Dy}_{0.04}\text{O}$ & $\text{Zn}_{0.85}\text{La}_{0.05}\text{Ce}_{0.05}\text{Dy}_{0.05}\text{O}$) under UV irradiation at different time intervals. (c) Photocatalytic degradation percentage of Rhodamine B dye solution with undoped ZnO and La, Ce, Dy co-doped ZnO nanoparticles ($\text{Zn}_{0.97}\text{La}_{0.01}\text{Ce}_{0.01}\text{Dy}_{0.01}\text{O}$, $\text{Zn}_{0.94}\text{La}_{0.02}\text{Ce}_{0.02}\text{Dy}_{0.02}\text{O}$, $\text{Zn}_{0.91}\text{La}_{0.03}\text{Ce}_{0.03}\text{Dy}_{0.03}\text{O}$, $\text{Zn}_{0.88}\text{La}_{0.04}\text{Ce}_{0.04}\text{Dy}_{0.04}\text{O}$ & $\text{Zn}_{0.85}\text{La}_{0.05}\text{Ce}_{0.05}\text{Dy}_{0.05}\text{O}$) under UV irradiation at different time intervals.
- 6) **Fig 6(a, b)** (a) Reflectance spectra of un-doped and $\text{Zn}_{0.97}\text{La}_{0.01}\text{Ce}_{0.01}\text{Dy}_{0.01}\text{O}$, $\text{Zn}_{0.91}\text{La}_{0.03}\text{Ce}_{0.03}\text{Dy}_{0.03}\text{O}$, & $\text{Zn}_{0.85}\text{La}_{0.05}\text{Ce}_{0.05}\text{Dy}_{0.05}\text{O}$ (b) Bandgap plot using the Kubelka–Munk function.
- 7) Table 1 Standard conditions for synthesis of La, Ce, Dy co-doped ZnO nanoparticles $x = (0.00-0.05)$
- 8) Table 2 Calculated lattice parameters and crystallite size of undoped and La, Ce, Dy co-doped ZnO nanoparticles